AN INVESTIGATION INTO THE AERODYNAMIC ROUGHNESS OF SEA SURFACE USING THE DATA FROM AN OFFSHORE METEOROLOGICAL TOWER

Y. H. Chen, J. J. Miau*, Y. R. Chen, C. Y. Lee, H. S. Chi, C. Y. Shang,
Department of Aeronautics and Astronautics
National Cheng Kung University
1, University Road, Tainan, Taiwan 70101
*Email: jjmiau@mail.ncku.edu.tw

D. J. Doong, Y. M. Fang
Costal Ocean Monitoring Center
National Cheng Kung University
1, University Road, Tainan, Taiwan 70101

Y. S. Tsai
Master Program in Offshore Wind Energy Engineering
National Kaohsiung University of Science and Technology, Kaohsiung, Taiwan 805301

J. C. Juang
Department of Electrical Engineering
National Cheng Kung University
1, University Road, Tainan, Taiwan 70101

ABSTRACT

A viscous flow analysis was carried out to examine sea surface roughness together with friction velocity using the data obtained from an offshore meteorological tower near Taichung harbor Taiwan. The data collected were during the northeast monsoon season that strong northeast wind was prevailing over the Taiwan strait. Specifically, this analysis was carried out from a viewpoint that the atmospheric boundary layer is roughened by surface waves. Thus, the surface layer could be described by a log velocity profile with the Nikuradse roughness length, k_s. A wall function was introduced in the momentum equation to evaluate the viscous force at the sea surface, which is equivalent to the pressure gradient force in the freestream. In practice, the quantity of k_s was determined through an iteration process satisfying an empirical relation between B and ${k_s}^+$ (Schlichting, 1968), where B denotes the constant in the log velocity profile originally describing turbulent flow through a rough pipe. It is found that the pressure gradient force reduced is in good agreement with that deduced from the high-resolution surface pressure map provided by Central Weather Administration Taiwan. In this study, a relation between k_s and friction velocity was obtained.

INTRODUCTION

Strong northeast wind prevails offshore the west coast of Taiwan during the winter time, which is primarily due to the high-pressure system developed at Mainland China and further strengthened by the terrain effect around Taiwan island. By taking the advantage of this nature resource, large-scale wind farm projects are being developed in the region.

A TGC meteorological tower situated offshore near the Taichung Harbor (24.048830ºN, 120.277139ºE) has been serving for the needs of local wind energy industry for almost one decade; GNC stands for Taiwan Generations Corporation. Recently, academic interests in using this met tower were inspired by the GNSS-R satellite remoting sensing realized by the TRITON space mission of TASA (Juang et al., 2024); TASA stands for Taiwan Space Agency.

This study was enabled with the instrument installed on the met tower including a GNSS-R antenna at the top 86m above the water surface, an ultrasonic anemometer 30 m above the water surface and four water gauges on the platform 18 m above the water surface.

The objective of this investigation is to explore the characteristics of sea surface roughness under high wind conditions, which is relevant to two aspects from the perspectives of application. One is concerned with wind energy harvested in the region which is known significantly intensified during the winter time, the other is concerned with the sea surface condition which can be inferred by the GNSS-R signals from the TRITON satellite. Hence, a comparison based on the ground-truth data obtained from the met tower and the remoting sensing data can be made.

As far as the GNSS Reflectometry (GNSS-R) is concerned, it can be briefly explained below. By comparing the GNSS signals received from the satellites and those reflected from the sea surface, the information of wind speed over the surface can be retrieved. (Garrison et al., 2002; Clarizia and Ruf, 2016; Juang et al., 2016) In principle, the higher the wind speed, the rougher the sea surface and the weaker the intensity of the GNSS-R signals received. In the method, the sea surface roughness is introduced with a quantity named mean-square-slope (MSS) of wave motions. (Hwang, 2022; Garrison et al., 2002; Cox and Monk, 1954)

A challenge realized in using this remote sensing method is how to minimize the uncertainty of wind speed retrieved, particularly at high wind speeds. Clearly, this issue is linked to the characteristics of surface roughness. (Hwang, 2022; Juang et al., 2024; Chen et al., 2025) Motivated by this concern, this study considered the roughness of sea surface in terms of k_s and z_0, therefore the air flow over the surface could be treated as a roughened turbulent boundary layer (Clauser, 1956). k_s denotes the Nikuradse's roughness length (Kadivar et al., 2021; Tennekes and Lumley, 1994; Schlichting, 1968; Clauser, 1956); z_0 denotes the characteristic roughness length in describing the log velocity profile of atmospheric boundary layers (Counihan, 1975; Wieringa, 1993; Garratt, 1994).

A viscous flow analysis on the atmospheric boundary layer was then carried out subjected to a neutrally stable condition at high wind speeds. In practice, an iteration process was employed to find the aerodynamic roughness together with friction velocity appropriate to a given wind speed, for which the exit criterion is that the flow quantities mentioned should satisfy an empirical relation concluded from the data of turbulent flows through roughened pipes. (Schlitching, 1968) Lastly, discussion is made concerning the sensitivities of k_s, z_0 and MSS to the friction velocity, a key quantity characterizing the atmospheric boundary layer.

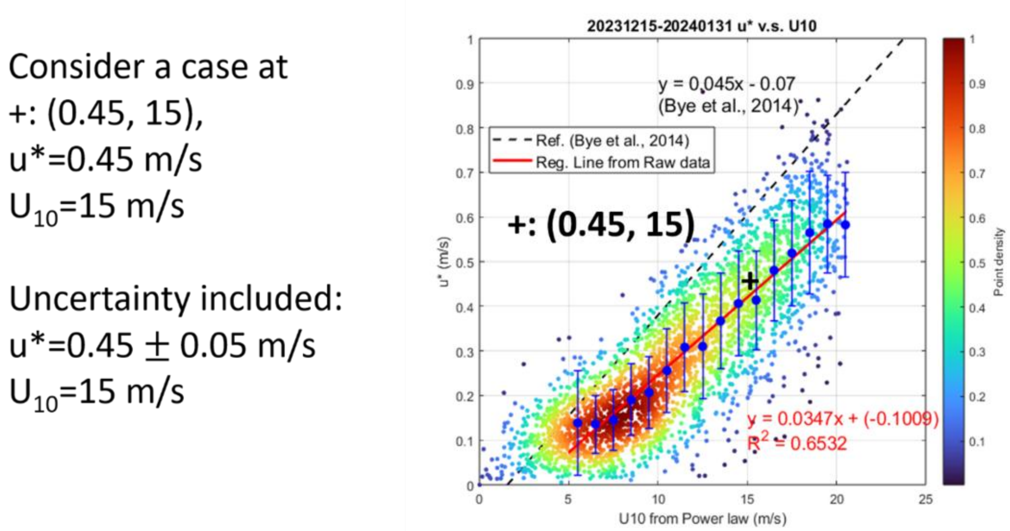

Figure 1. A plot of $u*$ versus U_{10} with two linear curves provided for reference, where U_{10} denotes the wind speed at 10 m above the water surface. U_{10} was extrapolated from the wind speed measured by the ultrasonic meter at 30 m above the water surface using the one-seventh power law. The data points marked in big dots indicate the mean values of $u*$ at the corresponding U_{10} wind speeds, each of which is accompanied with an uncertainty range. Half of the range corresponds to the root-mean-square value of the $u*$ data at the given wind speed.

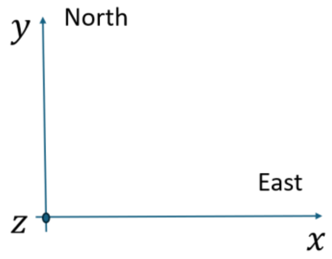

Figure 2. The rectangular coordinate system employed for this study; x and y are in the eastward and northward direction, respectively, and z denotes the elevation height, where $z = 0$ is at the water surface.

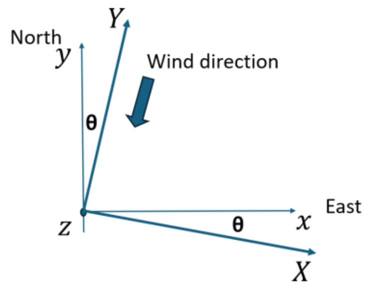

Figure 3. The coordinate system (X, Y, z) employed for describing the flow near $z = 0$. θ denotes the wind direction. Y is against the wind direction and X is normal to the wind direction.

Table 1. The results of cases: (a) $u*$=0.4 m/s; (b) $u*$=0.45 m/s ; (c) $u*$=0.5 m/s for U_{10}=15 m/s.

Case	u^*(m/s)	k_{s}(m)	z_0 (m)	$\frac{\partial p}{\partial x}$ (m/s²)	$\frac{\partial p}{\partial y}$ (m/s²)	fv (m/s²)	$-fu$ (m/s²)
a	0.4	10^{-5}	0.19x10^{-3}	(too large to be considered)	(too large to be considered)	-1x10^{-3}	0.6x10^{-3}
b	0.45	0.5x10^{-3}	0.24x10^{-3}	0.076	0.132	-1x10^{-3}	0.6x10^{-3}
c	0.5	1.85x10^{-3}	0.3x10^{-3}	5.5×10^{-3}	9.4×10^{-3}	-1x10^{-3}	0.6x10^{-3}

METHODOLOGY

Sea surface roughness cauesed by wave motions is primarily due to the shear stress of wind. (Stewart, 1976; Wu, 1980) In this study, the shear stress in terms of the friction velocity, u^*, was obtained from an ultrasonic anemometer on the meteorological tower.

A plot of u^*versus U_{10} is shown in Fig. 1, based on the data obtained during December 15, 2023 to January 31, 2024; U_{10} denotes the wind speed at 10 m above the water surface. U_{10} was extrapolated from the one-seventh power law using the wind speed data of the ultranonic anemomenter. Notably, the data in Fig. 1 show scattering substantially, particularly at high wind speeds. Two linear curves are included for reference, one of which was plotted according to Bye et al. (2014) and the other was obtained by linear regression based on the data in the plot. In the figure, the points marked in bigger dots indicate the mean values of u^* at the corresponding U_{10} wind speed, each of which is accompanied with an uncertainty range. Half the range indicates the root-mean-square value of u^*.

In the following, our efforts are focused on a viscous flow analysis on the atmospheric boundary layer at the site of the meteorological tower, which is assumed neutrally stable. Furthermore, the atmospheric boundary layer is assumed two-dimensional in the time mean sense. This assumption was validated once by comparing the scanning lidar data measurements made at Taichung Harbor and the data of a sounding balloon released from Penghu Island, 160 km west from the harbor, which showed a good consistency. More information learned from the comparison is that the atmospheric boundary layer was about 1 km thick, which was capped by an inversion layer of 0.7 km in thickness.

The two-dimensional, time-mean momentum equations describing the atmospheric boundary layer are shown below with the rectangular coordinate system defined in Fig. 2. The velocity components in the x, y and z directions are denoted as u, v and w, respectively, where z=0 denotes the elevation height at the water surface; f denotes the Coriolis parameter; p denotes the static pressure of air; ν and ρ denote the kinematic viscosity and density of air, respectively.

$$\frac{Du}{Dt} = fv - \frac{\partial p}{\partial x} + (Reynolds\ stress) + \nu\frac{\partial^2 u}{\partial z^2} \quad (1)$$

$$\frac{Dv}{Dt} = -fu - \frac{\partial p}{\partial y} + (Reynolds\ stress) + \nu\frac{\partial^2 v}{\partial z^2} \quad (2)$$

In the freestream of the boundary layer, the momentum equations (1) and (2) can be simplified by ignoring the contributions of Reynolds stresses and viscous stresses.

At z=0, the shear stress is in the direction of the pressure gradient. For convenience, (1) and (2) can be combined into one equation with the coordinate system re-defined in Fig. 3, that the wind is along the negative Y dirction. Along the wind direction, the total wind speed is denoted as U : $U = (u^2 + v^2)^{1/2}$. Therefore, the momentum equation in the direction Y can be written below.

$$0 = -\frac{\partial p}{\partial Y} + \nu \frac{\partial^2 U}{\partial z^2}_{(at\ z=0)} \quad (3)$$

To evaluate the viscous term in (3), a wall function is needed to describe the transition from the linear profile at z=0 to the log profile in surface layer.

$$\text{At } z = 0\text{: } U^+ = z^+;\ U^+ = \frac{U}{u^*},\ z^+ = z/k_s \quad (4)$$

In (4), u^* and k_s are employed for the normalization of U and z, respectively.

In the surface layer, the velocity profile is represented by a log profile in (5) with the von Karman constant k =0.4 and B being a constant. (Schlichting 1968) B depends on the surface roughness; B =8.5 if completely rough for ${k_s}^+ > 70$, where ${k_s}^+ = k_s u^*/\nu$. (Schlichting, 1968).

$$U^+ = (1/k)\ln z^+ + \mathrm{B} \quad (5)$$

In viewing that this study is focused on high-wind situations, B is assumed 8.5 initially.

To smoothen the velocity profile at small z, a correction term is needed to modify the linear profile (4). Referring to Spalding (1961), the correction form is suggested as follows.

$$z^+ = U^+ + 0.033\left(e^{0.4U^+} - 1 - 0.4U^+\right) \quad (6)$$

where $\left(e^{0.4U^+} - 1 - 0.4U^+\right) = \frac{(0.4U^+)^2}{2!} + \frac{(0.4U^+)^3}{3!} + \frac{(0.4U^+)^4}{4!} + \ldots$ (7)

As seen in (6), the near-wall velocity profile is expressed as $z^+ = z^+(U^+)$, instead of $U^+ = U^+(z^+)$. The correction term in (6) is dominated by the leading term of U^{+2} for U^+ being small. Subsequently, evaluation on the viscous force term at z =0 can be carried out.

$$\frac{d^2 U}{d^2 z}_{(at\ z^+=0)} = -0.00528\ \frac{u^*}{{k_s}^2} \quad (8)$$

In (8), with u^* and k_s known, evaluation on the viscous force term at $z = 0$ is enabled.

It is noteworthy that the pressure gradient at $z = 0$ is equivalent to the pressure gradient in the freestream. Subsequently, a momentum budget analysis for flow in the freestream in the x and y directions can be carried out.

A SAMPLE CASE OF THE PRESENT ANALYSIS

To illustrate the procedure above, a data set indicated Fig. 1 of u^*=0.45 m/s and U_{10}=15 m/s was selected. Further, an uncertainty range of u^*=0.45 $\pm$ 0.05 m/s was considered. Additional information needed was the wind direction θ=30°, and the freestream wind speed was 22.8 m/s at z=200 m, which was determined by an extrapolation using the one-seventh power law.

The results of the cases: (a) u^*=0.4 m/s; (b) u^*=0.45 m/s ; (c) u^*=0.5 m/s for U_{10}=15 m/s are given in Table 1. Note that k_s was determined according to (5) with B =8.5; z_0 was reduced using the Charnock relation below (Charnock, 1955), where g is the gravity.

$$\frac{z_0 \mathrm{g}}{u^{*2}} = \text{constant} \quad (9)$$

The constant value in (9) was chosen 0.012 (Peña and Gryning, 2017). It is seen in the table that the variations of z_0 over the three cases are relatively insensitive to u^*, compared to those of k_s. This issue will be further discussed later.

In Table 1, the pressure gradient force of case (a) is too large to be physically possible. Therefore, only cases (b) and (c) are further considered.

In either of case (b) or (c) the pressure gradient force is greater than the Coriolis force estimated. This comparison infers that in the freestream the pressure gradient force is dominant over the Coriolis force.

The k_s^+ value of case (c) is larger than that of case (b), but still less than 70. This signifies that the initial assumption of the atmospheric boundary layer being fully roughened would not be adquate, and is required re-examination. In practice, an iteration process was undertaken with the constant B in (5) being adjustable. The exit criterion was that a set of B and k_s^+ determined should be complied with an empirical relation concluded from the data of turbulent flows through roughened pipes. (Schlichting, 1968)

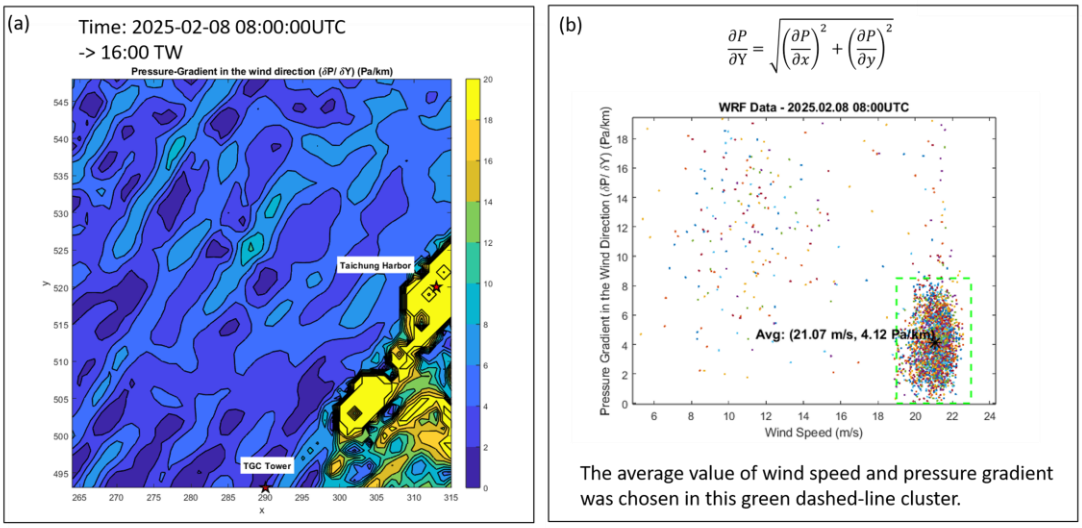

Figure 4. WRF numerical simulation – Pressure Gradient in the wind direction. (a) Surface pressure map offshore Taichung harbor; (b) distribution of the values of pressure gradient estimated at the grid points of the grid size 1 km by 1 km in the map.

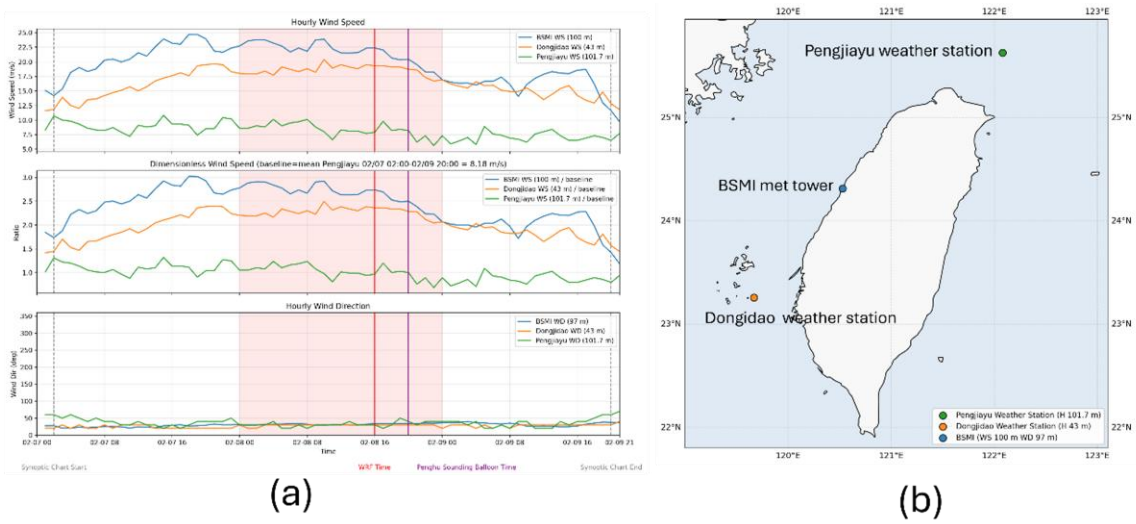

Figure 5. Comparison of the hourly wind data at Pengjiayu weather station (CWA), Donggido weather station (CWA) and BSMI met tower at Taichung harbor during a Monsoon period of February 7 to 9, 2028; BSMI stands for Bureau of Standards, Metrology and Inspection. In (a), the top plot shows the data of wind speed (m/s); the middle plat shows the wind speed data normalized by 8.18 m/s, the time mean speed at Pengjiayu weather station over the period of the two days; the bottom plot shows that the wind directions corresponding to the wind speeds measured at the three locations. In (b), the map of Taiwan with the geographical locations of the three met towers indicated.

For the present case, U_{10}= 15 m/s, u^* and k_s determined from the iteration process are 0.52 m/s and 2.93 mm, respectively; ${k_s}^+$ is about 95, which is confirmed in the fully-roughened regime. Meanwhile, the pressure gradient obtained from (3) is 4.8 Pa/km or 4.8x10^{-3} m/s^2, which is found in good agreement with that deduced from the high-resolution surface pressure map provided by Central Weather Administration. More details in this regard are provided in the section below.

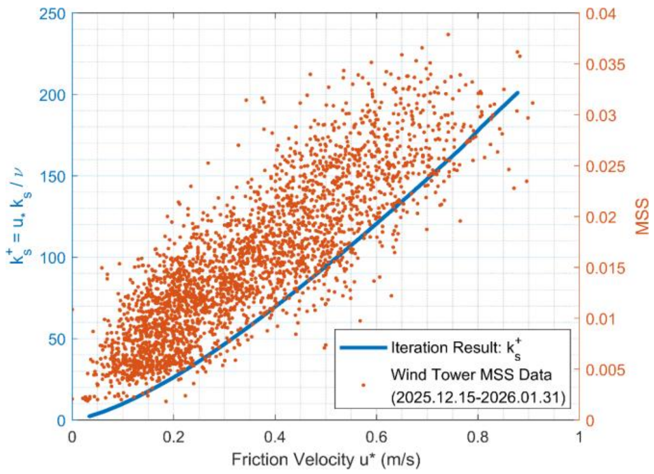

Figure 6. A plot of ${k_s}^+$ and MSS versus u^*. The vertical scale on the left indicates ${k_s}^+$ for the values resolved from the present viscous flow analysis; the vertical scale on the right indicates MSS, for which the data were resolved from the wave gauges on the met tower.

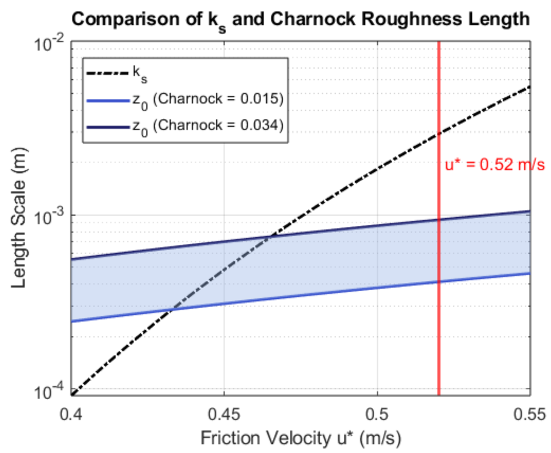

Figure 7. A plot of k_s and z_0 versus u^*. The red line at u^*=0.52 m/s marks the sample case of U_{10} = 15 m/s considered in the present analysis.

DISCUSSION

Figure 4a shows the high-resolution surface pressure map obtained by WRF numerical simulation at 4pm, February 8, 2025 (Taiwan time) in the region offshore Taichung harbor; WRF stands for the Weather Research Forecasting model which is an open source software for weather prediction. Figure 4b provides the distribution of the values of pressure gradient in Pa/km estimated at the grid points in the map of a grid size of 1 km by 1 km versus the local wind speed. As seen in Fig. 4b, the data points are highly clustered in a wind speed range of 19 m/s to 22 m/s, where can be realized from Fig. 4a in the proximity of Taichung Harbor. It is noteworthy that the wind speed range is consistent with that of the free stream of the atmospheric boundary layer in the sample case presented in the previous section. Further, by averaging over the pressure gradient values within the green box indicated in the figure, the mean value is 4.12 Pa/km, which is close to 4.8 Pa/km resolved from the viscous flow analysis in the sample case. This agreement gives a strong support to the validity of the present viscous analysis.

The pressure gradient force in the region is noted substantially higher than that would have been due to the synoptic weather system. Physically speaking, in the geostropic wind layer, the pressure gradient force would be balanced by the Coriolis force in the order of 1 Pa/km. For instance, the pressure gradient force associated with the high- and low-pressure circulations in the north Atlantic Ocean falls in the order of 1 Pa/km. (Hurrell, 1995.; Kastendeuch, 2007) In the atmospheric boundary layer of the present concern, that the pressure gradient force is significantly higher than the Coriolis force is primarily due to the terrain effect. In fact, as the northeast wind prevailing over Taiwan island, Taichung harbor is situated at the leeside of the Central Mountain Range, whose elevation reaches almost 4000 m at the highest.

The terrain effect can also be learned by other sources of wind data. Figure 5 compares the wind data obtained from three met towers around Taiwan island during a time period of February 7-9, 2025. In the figure, it is clearly seen that at 4pm, February 8, the wind speed at Taichung harbor was more than two times that at Pengjiayu weather station, the location north of Taiwan where was supposedly suffered little impact from the terrain effect. The third location Donggido weather station situated in Taiwan Strait was suffered similar terrain effect but less than that at Taichung harbor.

A discussion on ${k_s}^+$ and MSS is made with Fig. 6, both of which are non-dimensional quantities varied with u^*. The curve of ${k_s}^+$ was obtained from the present viscous flow analysis, and the MSS data were deduced from the water gauges on the TGC met tower. The latter show scattering somewhat, nevertheless a trend revealed consistently is that it is increased with u^*.

Both quantities of ${k_s}^+$ and MSS characterize the roughness of sea surface. It is proposed here that ${k_s}^+$ could be an option for MSS in retrieving the wind speed from the signals of GNSS-R with reasoning below. In Fig. 6, it is seen that ${k_s}^+$ is ranged between 0 and 200 whereas MSS is ranged between 0 and 0.04, for u^* between 0 to 0.9 m/s. Therefore, in terms of the sensitivities of ${k_s}^+$ and MSS to u^*, the former is 5000 times the latter. The advantage of ${k_s}^+$ over MSS in retrieving the wind speed is evident from the comparison.

Further discussion on k_s and z_0 versus u^* is made below with Fig. 7, in which u^* is ranged between 0.4 to 0.55 m/s of the present interest. Concerning the sensitivities of k_s and z_0 to u^*, this figure unveils that the slopes of k_s and z_0 are differed remarkably. In the figure, the vertical axis is scaled logarithmic in meter. The values of z_0 fall within a band since the Charnock constant in (9) reported in the literature were varied in a range (Charnock, 1955; Garratt, 1977; Wu, 1980; Johnson et al., 1998). Literally speaking, z_0 appears much less sensitive to u^* than k_s does. In a concern of retrieving the wind speed, using k_s is evidently superior over using z_0.

CONCLUDING REMARKS

Two contributions of this study can be stated below. First, a viscous flow analysis was employed for a roughened turbulent boundary layer simulating the atmospheric boundary layer over a sea surface at high wind, which led to the determination of u^* and k_s at a given U_{10}. It is noteworthy that the analysis was enabled with a wall function and an iteration process. Moreover, referring to the sample case of U_{10}= 15 m/s, the pressure gradient force determined in the free stream was found in good agreement with that deduced from the high resolution surface pressure map. Second, a comparison on the surface roughness quantities of k_s, z_0 and MSS was made, from which it was concluded that k_s is the most sensitive one to u^*. This finding has a significance in that ${k_s}^+$ could be considered as an option for MSS in retrieving the information of wind speed over sea surface from the GNSS-R signals.

The Nikuradse roughness length, k_s, originally was introduced to describe turbulent flows through rough pipes. (Schlichting, 1968) Subsequently, it was validated for turbulent boundary layers over roughened surfaces. (Clauser, 1956) Physically, it is a length scale characterizing flow in the inner region of a wall-bounded turbulent shear flow, irrespective of the outer region. (Tennekes and Lumley 1972) The present study successfully extended the use of this roughness parameter to describe a neutrally-stable atmospheric boundary layer roughening sea surface.

ACKNOWLEDGMENT

Authors would like to acknowledge Central Weather Administration for using their scanning lidar during February to April 2025 at Taichung Harbor, and kindly providing the high-resolution surface pressure map at 4pm on February 8, 2025. Acknowledgment also goes to Taiwan Generations Corporation for using their offshore met tower to collect the wind, wave and GNSS-R data. Funding support for this study from TASA under the contract number: TASA-S-1130505 is greatly appreciated.

REFERENCES

Bye, J. A. T., Wolff, J. O., and Lettmann, K A., 2014, “On the Variability of the Charnock Constant and the Functional Dependence of the Dag Coefficient on Wind Speed: Part II-Observations”, *Ocean Dynamics* Vol. 64, pp. 969–974.

Charnock, H., 1955, “Wind Stress on a Water Surface”, *Quarterly Journal of the Royal Meteorology Society*, Vol. 81, Issue 350, pp. 639-640.

Chen, M. Y., Chien, H., Yeh, W. H., Lin, L. C., and Liou, Y. F., 2025, “Evaluation of the Effect of Satellite Motion on GNSS-R Wind Speed Retrieval: Insights from TRITON”, *Frontiers in Remote sensing*, 30 July 2025. DOI 10.3389/frsen.2025.1657576.

Clarizia, M. P. and Ruf, C. S., 2016, “Wind Speed Retrieval Algorithm for the Cyclone Global Navigation Satellite System (CYGNSS) Mission”, *IEEE Transctions on Geoscience and Remote Sensing*, Vol. 54, No. 8, August 2016, pp. 4419-4432.

Clauser, F. H., 1956, “The Turbulent Boundary Layer”, *Advances in Applied Mechanics*, Vol. 4, pp. 1-51.

Cox, C. S., and Munk, W., 1954, “Statistics of the Sea Surface Derived from Sun Glitter”, *J. Mar. Res.*, Vol. 13, pp. 198-227.

Counihan, J., 1975, “Adiabatic Atmospheric Boundary Layers: a Review and Analysis of Data from the Period of 1880-1972”, *Atmospheric Environment*, Vol. 9, Issue 10, pp. 871-905.

Garratt, J. R., 1977, “Review of Drag Coefficients over Oceans and Continents”. *Mon. Wea. Rev.*, Vol. 105, pp. 915-929.

Garratt, J.R., 1994, “Review: the Atmospheric Boundary Layer”, *Earth-Science Reviews*, Vol. 37, pp. 89-134.

Garrison, J. L., Komjathy, A., Zavorotny, V. U., and Katzberg, S. J. 2002, “Wind Speed Measurement Using Forward Scattered GPS Signals”, *IEEE Transactions on Geoscience and Remote Sensing*, Vol. 40, No. 1, pp. 50-65.

Hurrell J.W., 1995, “Decadal Trends in the North Atlantic Oscillation: Regional Temperatures And Precipitation”, *Science*, Vol. 269, pp. 676–679.

Hwang, P. A., 2022, “Ocean Surface Roughness from Satellite Observations and Spectrum Modeling of Wind Waves”, *Journal of Physical Oceanography*, Vol. 52, pp. 2143-2158. DOI: 10.1175/JPO-D-22-0043.1

Johnson, H. K., Højstrup, J., Vested, H. J., Larsenon, S. E., 1988, “The Dependence of Sea Surface Roughness on Wind Waves”, *Journal of Physical Oceanography*, Vol. 28, pp.1702-1716.

Juang, J. C., Ma, S. H. and Lin, C. T., 2016, “Study of GNSS-R Techniques for FORMOSAT Mission,” *IEEE Journal of Selected Topics in Applied Earth Observations and Remote Sensing*, Vol. 9, No. 10, pp. 4582-4592. doi:10.1109/JSTARS.2016.2575069.

Juang, J.-C., Tsai, Y.-F., and Lin, C.-T., 2024, “TRITON GNSS-R Mission: Preliminary Results and Perspectives”, *IGARSS 2024 - 2024 IEEE international geoscience and remote sensing symposium*, Athens, Greece: IEEE. p. 6725–6728. doi:10.1109/igarss53475.2024.10642499

Kadivar, M., Tormey, D., McGranaghan, G., 2021, “A Review on Turbulent Flow over Rough Surfaces: Fundamentals and Theories”, *International Journal of Thermofluids*, Vol. 10, 100077.

Kastendeuch, P. P., 2007, “Pressure Gradient Force, Atmospheric Circulation and Climate in Western Europe (1899–2002)”, *Int. J. Climatol.*, Vol. 27, pp. 2055–2067.

Peña, A,. Gryning, S. E., 2008, “Charnock’s Roughness Length Model and Non-dimensional Wind Profiles Over the Sea,” *Boundary-Layer Meteorology*, Vol. 128, pp. 191–203.

Schlichting, H., 1968, *Boundary-Layer Theory*, translated by J. Kestin, Sixth Edition, McGraw-Hill, Inc.

Spalding, D. B., 1961, “A Single Formula for the Law of the Wall”, *Transactions of the ASME*, September 1961, pp. 456-457.

Stewart, R. W., 1976, “The Air-Sea Momentum Exchange”, *Boundary-Layer Meteorology*, Vol. 6. pp. 151-167.

Tennekes, H., and Lumley, J. L., 1994, *A First Course in Turbulence*, in Chapter 5: Wall bounded shear flows, The MIT Press.

Wieringa, J., 1993, “Representative roughness parameters for homogeneous terrain”, *Boundary-Layer Meteorology*, Vol. 63, pp. 323-363.

Wu, J., 1980, “Wind-Stress Coefficients over Sea Surface near Neutral Conditions, a Revisit”, *Journal of Physical Oceanography*, Vol. 10, pp. 727-740.